Article

mRNA trans-splicing dual AAV vectors for (epi)genome editing and gene therapy

Lisa Maria Riedmayr [1], Klara Sonnie Hinrichsmeyer [1],
Stefan Bernhard Thalhammer[1], David Manuel Mittas[1], Nina Karguth[1],
Dina Yehia Otify[1], Sybille Böhm[2], Valentin Johannes Weber[3],
Michael David Bartoschek [2], Victoria Splith[2], Manuela Brümmer[1],
Raphael Ferreira[4], Nanda Boon [5], Gabriele Maria Wögenstein[6],
Christian Grimm [6], Jan Wijnholds [5,7], Verena Mehlfeld[1], Stylianos Michalakis[8],
Stefanie Fenske [1,9], Martin Biel[1] & Elvir Becirovic [3] ✉

Large genes including several CRISPR-Cas modules like gene activators (CRISPRa) require dual adeno-associated viral (AAV) vectors for an efficient in vivo delivery and expression. Current dual AAV vector approaches have important limitations, e.g., low reconstitution efficiency, production of alien proteins, or low flexibility in split site selection. Here, we present a dual AAV vector technology based on reconstitution via mRNA trans-splicing (REVeRT). REVeRT is flexible in split site selection and can efficiently reconstitute different split genes in numerous in vitro models, in human organoids, and in vivo. Furthermore, REVeRT can functionally reconstitute a CRISPRa module targeting genes in various mouse tissues and organs in single or multiplexed approaches upon different routes of administration. Finally, REVeRT enabled the reconstitution of full-length ABCA4 after intravitreal injection in a mouse model of Stargardt disease. Due to its flexibility and efficiency REVeRT harbors great potential for basic research and clinical applications.

Adeno-associated virus (AAV)-mediated gene transfer is the most efficient and widely used method for in vivo gene delivery in mammals[1,2]. Despite numerous advantages over other therapeutic vectors (e.g., low overall pathogenicity and toxicity and ability to transduce non-dividing cells), AAVs have an important limitation: their low genome packaging capacity of 4.7–5.0 kb[3]. This hampers their use for the expression of large genes including many therapeutically relevant CRISPR-Cas9 modules, such as gene activators (CRISPRa), gene inhibitors (CRISPRi), and base or prime editors[2,4]. To overcome this constraint, several strategies have been established following the

same principle: The gene of interest is split into two parts and packaged into separate AAV vectors, typically referred to as dual AAVs. Depending on the approach, the split parts of the gene can subsequently be reconstituted at the AAV genome, mRNA, or protein level upon co-delivery of the dual AAVs to the target tissue[2,5].

Gene reconstitution at the AAV genome level (from here on referred to as DNA trans-splicing) was the first dual AAV vector approach applied in vivo. The different versions of this method rely on homologous recombination and/or concatemerization of the AAV genome[6–9]. However, DNA trans-splicing often results in low to

---

[1]Department of Pharmacy - Center for Drug Research, LMU Munich, Munich 81377, Germany. [2]ViGeneron GmbH, Planegg 82152, Germany. [3]Laboratory for Retinal Gene Therapy, Department of Ophthalmology, University Hospital Zurich, University of Zurich, Schlieren 8952, Switzerland. [4]Genetics Department, Harvard Medical School, Boston, MA 02115, USA. [5]Department of Ophthalmology, Leiden University Medical Center (LUMC), 2333 ZA Leiden, Netherlands. [6]Laboratory for Retinal Cell Biology, Department of Ophthalmology, University Hospital Zurich, University of Zurich, Schlieren 8952, Switzerland. [7]Netherlands Institute for Neuroscience, Institute of the Royal Netherlands Academy of Arts and Sciences (KNAW), 1105 BA Amsterdam, Netherlands. [8]Department of Ophthalmology, University Hospital, LMU Munich, 80336 Munich, Germany. [9]German Center for Cardiovascular Research (DZHK), partner site Munich Heart Alliance, Munich 81377, Germany. ✉e-mail: elvir.becirovic@uzh.ch

moderate reconstitution efficiency[10–13]. By comparison, the split intein approach operates at the protein level and, if successful, typically leads to high reconstitution efficiencies[11,12,14–17]. Nevertheless, as it requires proper protein folding of both split fragments, this method strongly depends on the split position and relies on the presence of specific amino acids within the split site[18,19]. Therefore, finding a suitable and efficient split position requires an elaborate and time-consuming screening process for each gene and might fail completely. In addition to its low flexibility, this approach creates equimolar amounts of potentially immunogenic or pathogenic proteins (inteins), raising important safety concerns for translational approaches. This may become even more relevant if split inteins are combined with Cas-based technologies, given that a co-expression could enhance host immune response in an additive or synergistic manner.

Consequently, there is a high unmet need for a strategy that overcomes the limitations of the current gene reconstitution approaches. Reconstitution via dual mRNA trans-splicing AAVs remains a largely unexplored option. To date, mRNA trans-splicing in combination with AAVs has been used to express the cystic fibrosis transmembrane conductance regulator (*CFTR*) gene in a single study in cell culture experiments[20]. Nevertheless, it was barely optimized in its safety or efficiency and has yet to be effectively employed in vivo, in disease models and in gene editing approaches. Despite utilizing similar sequence elements as DNA trans-splicing (e.g., complementary domains and splice sites), the reconstitution in the mRNA trans-splicing approach occurs between two different mRNA molecules, i.e., in *trans*[21]. Thus, it is fundamentally different from DNA trans-splicing, in which mRNA splicing occurs in *cis* with the sole purpose of removing the non-coding portions between the split fragments after successful reconstitution at the genome level. Nevertheless, in many studies, dual DNA trans-splicing AAV vectors have been incompletely termed trans-splicing[22–24] or were even mixed up with mRNA trans-splicing approaches[11]. This unfavorable terminology makes it difficult for non-experts to distinguish between the respective methods.

Here, we develop a flexible and efficient dual AAV vector-based method utilizing mRNA trans-splicing for the reconstitution of large coding sequences. These vectors have been tested in the context of various therapeutically highly relevant genes or gene editing modules in a variety of challenging experimental setups in vitro and in vivo.

Results

Development of REVeRT technology for reporter gene reconstitution in vitro

To test and optimize REVeRT, we developed a split-fluorophore assay that results in the expression of cerulean, a cyan fluorescent protein, upon successful reconstitution of the two split fragments (Fig. 1a). For this experiment, we used the CAG|GT sequence as a split site for REVeRT with the vertical line symbolizing the split point. This sequence is derived from the exonic part of the splice site consensus sequence, i.e., CAG marking the end of an exon at the splice donor site and a G the start of an exon at the splice acceptor site. The T at the last position is part of the exonic sequence of a very strong splice acceptor published in our recent study[25]. The CAGGT sequence cannot be found within the short (720 bp) native cerulean coding sequence. However, this sequence can be easily created by using synonymous codons without changing the protein code (Fig. S1a, split site #1).

Both split fragments were equipped with elements required for transcript expression and subsequent mRNA trans-splicing, i.e., promoter, complementary binding domains, splice sites, and polyadenylation signal. For initial testing, we used binding domain sequences of different lengths derived from the intronic sequence of the human rhodopsin (*RHO*) gene (Fig. S1b). Native intronic sequences typically contain intronic splicing enhancers that may facilitate mRNA trans-splicing-mediated reconstitution. We examined the principal

reconstitution capability of mRNA trans-splicing in transfected HEK293 cells and found that it results in a seamless, precise, and efficient ligation of the two fragments (Fig. 1b–e). Nevertheless, although helpful at this initial stage, human-derived sequences as binding domains are less suitable for translational approaches, as they are expected to bind to the respective human transcripts increasing the risk of off-target effects. Therefore, we tested additional binding domains derived from a 100 bp sequence of the bacterial *lacZ* gene that was modified to create four distinct binding domain sequences without any homology to the human or mouse genome. Moreover, the binding domains were designed to contain no suitable start codons that would facilitate the expression of artificial proteins or initiate an in-frame translation of the 3' coding sequence. One of them resulted in the highest reconstitution efficiency observed (44.0% in flow cytometry and 53.5 % in western blot-based quantifications, Fig. 1f, g and Table S1) and was therefore considered as the optimized binding domain for further experiments.

Next, we analyzed other trans-splicing elements for their effect on the reconstitution efficiency, i.e., position of the split site, presence of the polyadenylation signal, and strength of splice sites (Fig. 1h–k and Fig. S1c, d). An element showing a high impact on the reconstitution efficiency was the splice acceptor site (SAS). When comparing three different SASs predicted to be strong using splice site prediction software, efficient reconstitution was only observed for one SAS variant (Fig. 1h, i). This SAS was recently shown to be highly effective in different conditions[25]. Compared to the SAS, the splice donor site (SDS) showed a less pronounced effect as well as the presence of a polyadenylation signal (Fig. 1j, k). No cerulean reconstitution was observed when the promoter was removed from the 3' split fragment (v2) (Fig. 1j, k). This suggests that reconstitution is driven exclusively by mRNA trans-splicing and not via processes which occur at the DNA level such as homologous recombination. In another set of experiments, we show that different split sites lacking a C at the first and/or T at the last position of the CAGGT sequence all lead to a successful reconstitution yielding moderate to high expression levels (Fig. S1c, d). This indicates that AGG is the minimal split site consensus sequence for REVeRT. Moreover, REVeRT can be used for a directional reconstitution of the fluorophore sequence split into three fragments facilitated by two different binding domains (Fig. S1e, f) and is independent of the cell type (Fig. S1g, h).

Conclusively, in this part of the study, we identified and optimized several molecular determinants that affect the efficiency of REVeRT. These optimized elements (Table S2) were used for all subsequent experiments.

Evaluation of dual REVeRT AAVs in vivo

Next, we analyzed the performance of REVeRT in a dual AAV vector setting in vivo. The retina is the target organ of one of the first approved AAV gene therapies and for many others currently in clinical development[26,27]. However, more than 30 inherited retinal disorders are caused by mutations in large genes exceeding the AAV vector DNA capacity (https://sph.uth.edu/retnet/). We therefore evaluated the functionality of REVeRT in retinal cells by injecting two different split fluorophore variants into the eyes of C57BL/6J wild-type (WT) mice using AAV8(Y733F) vectors (Fig. S2a, b)[28]. The first variant expressing the split cerulean cassette was injected subretinally to target photoreceptors. The second variant contains one additional fluorophore, citrine or mCherry, fused directly to the split fragments to monitor the expression of the individual vectors and was injected under the monolayer of retinal pigment epithelial (RPE) cells. Additional start and stop codons not contained in the original REVeRT sequences have been added to citrine and mCherry to be able to track the expression of the single vectors. Four weeks after injection, both approaches showed robust and specific fluorophore expression in the respective target cells (Fig. S2c–e).
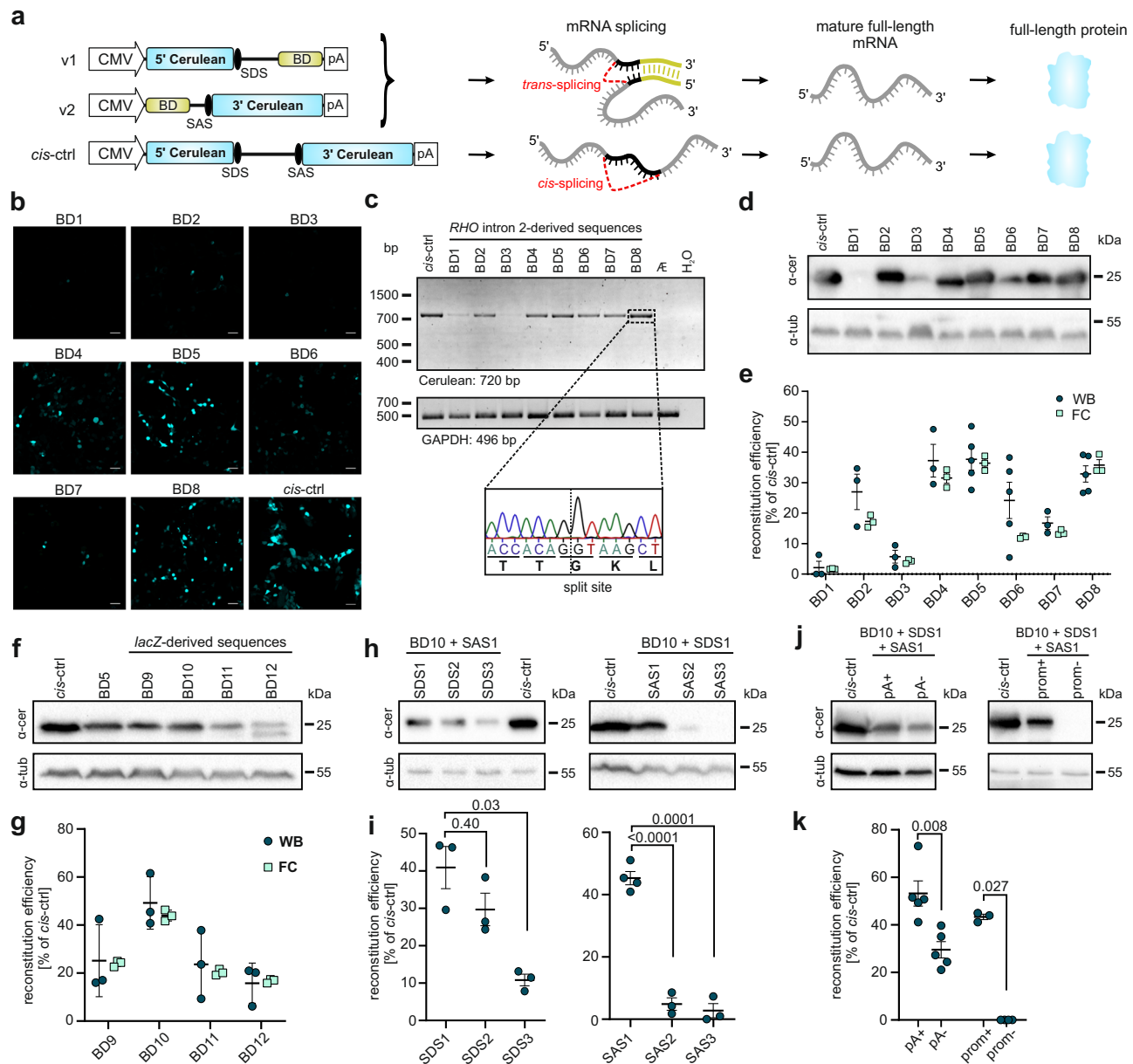
Fig. 1 | Development and optimization of mRNA trans-splicing in vitro.
a Illustration of split fluorophore assay to test reconstitution via mRNA trans-splicing. A cis-splicing vector served as positive control (cis-ctrl). v1, vector 1; v2, vector 2; BD, binding domain; SDS, splice donor site; SAS, splice acceptor site; pA, polyadenylation signal. **b** Confocal images of HEK293 cells transfected with v1 and v2 containing different BDs. Scale bar: 50 μm. **c** RT-PCR of reconstituted full-length cerulean. GAPDH served as input reference. Sequencing result of the splicing junction shown below. bp, base pairs. **d** Western blots of transfected cells shown in (**b**). α-cer, anti-cerulean antibody; α-tub, anti-β-tubulin antibody; kDa, kilodalton. **e** Quantification of reconstitution efficiency relative to cis-ctrl using western blots (WB, minimum of $n = 3$) or flow cytometry (FC, $n = 3$). **f** Western blot of cells transfected with v1 and v2 containing different human (*RHO* intron 2-derived, BD 5) or bacterial (*lacZ*-derived, BD 9–12) binding domains. **g** Ratiometric quantification

of reconstitution efficiency of the transfections shown in (**f**) relative to cis-ctrl. $n = 3$. **h** Western blots of cells transfected with v1 and v2 containing different SDS or SAS. **i** Ratiometric quantification of reconstitution efficiencies relative to cis-ctrl. $n = 3$. Welch's ANOVA with Dunnett T3 (SAS) or Kruskal-Wallis test with Dunnett T3 (SDS) was used. **j** Western blots of cells transfected with versions of v1 containing (+pA) or lacking (−pA) a polyadenylation signal and with versions of v2 containing (+prom) or lacking (−prom) a promoter. **k** Ratiometric quantification of reconstitution efficiencies relative to cis-ctrl. $n = 5$ (pA), $n = 3$ (prom). Two-tailed Mann–Whitney test was used. Scatter plots show mean ± SEM. For all co-transfections equimolar amounts have been used (1 μmol v1 + 1 μmol v2, corresponding to 1 μmol cis-ctrl). All 'n' in Fig. 1 represent independent transfections. All source data are provided as a Source Data file.

Next, to monitor REVeRT-mediated reconstitution in different organs, we developed a split luciferase reporter system. Three different split sites in the luciferase sequence were tested in vitro (Fig. S3). In line with the split cerulean assay, the different split sites showed only minor differences in reconstitution efficiency, further underlining the high flexibility of REVeRT in the split site selection. No luciferase signal was obtained for single split vectors (Fig. S3b). We used the REVeRT luciferase system to evaluate the reconstitution efficiency in different

organs upon intraperitoneal application. These are very challenging conditions considering that AAVs are diluted in the bloodstream, have to cross several biological barriers, and co-transduce the same cells before mRNA trans-splicing can occur. Three weeks after injecting dual AAV9 vectors into WT mice, luciferase signal was detectable throughout the body (Fig. 2a, b). The reconstituted luciferase was expressed in various organs of the injected animals with the strongest signal detectable in the heart (Fig. 2c). Moreover, we subretinally
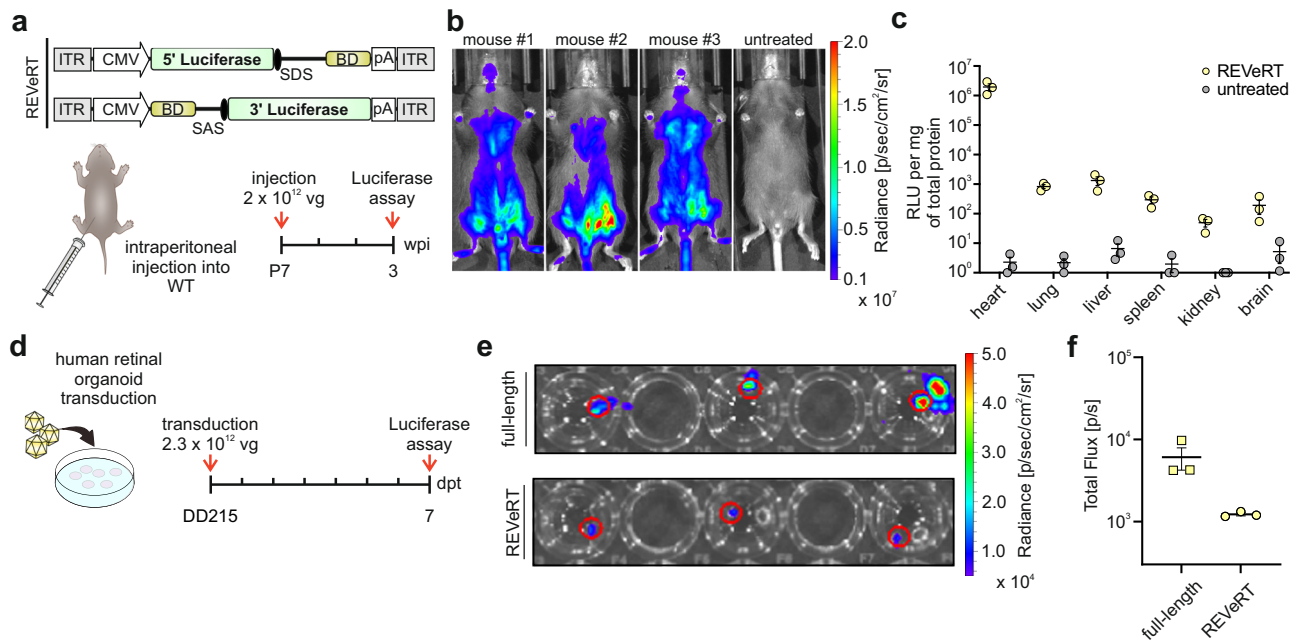
Fig. 2 | Reconstitution of luciferase via dual REVeRT AAVs in vivo and in human retinal organoids. a Dual REVeRT AAVs expressing a split luciferase gene. Lower panel, Time scale for experiments in WT mice (**b**, **c**). **b** Luminescence obtained from WT mice co-injected with titer-matched dual REVeRT AAV9 vectors. Untreated mice injected with luciferin served as negative control. **c** Relative quantification of luciferase expression in different organs three weeks post-injection. $n = 3$ mice. RLU, relative light units. **d** Time scale for experiments in human retinal organoids transduced with dual REVeRT AAV9 vectors at differentiation day 215 (DD215). dpt, days post-transduction. **e** Luminescence obtained from transduced organoids. Regions of interest indicating the organoid position were used for quantification and are shown in red. A AAV vector expressing full-length luciferase served as positive control. **f** Quantification of the results shown in (**e**). $n = 3$ retinal organoids. Scatter plots show mean ± SEM. All source data in this figure are provided as a Source Data file.

injected wildtype mice with split and full-length luciferase constructs. Compared to its full-length counterpart, the split REVeRT luciferase resulted in an average reconstitution efficiency of 25.5 ± 3.6% (Fig. S3d, e).

Collectively, these results show that dual REVeRT AAVs lead to the reconstitution of several split reporter genes in mice after local or systemic application of different AAV capsids.

Evaluation of dual REVeRT AAVs in human retinal organoids

To better assess the translational potential of dual REVeRT AAVs, we used human retinal organoids, which are frequently employed to evaluate the potency of therapeutic AAV vectors. To this end, we co-transduced human retinal organoids with AAV9 vectors carrying the split luciferase gene (Fig. 2d). The reconstituted luciferase reached 20.2 % of the signal from control organoids transduced with single AAVs expressing the full-length luciferase (Fig. 2e, f). This demonstrates that dual REVeRT AAVs can be used to transduce highly differentiated human tissue cultures.

Dual REVeRT AAVs result in functional reconstitution of dCas9-VPR in vitro and in vivo

Having studied the efficacy of REVeRT using reporter assays, we set out to evaluate this technology in a therapeutically relevant context. For this purpose, we focused on "dead" (d)Cas9 fused to VP64, p65, and Rta (VPR), a very potent CRISPRa module with high translational potential[29]. The range of applications of CRISPRa for the treatment of genetic or acquired diseases includes transcriptional activation (transactivation) of silent genes that are functionally equivalent to defective genes[30]. The *MYO7A* (*USH1B*) gene represents an attractive target for CRISPRa therapy, as it exceeds the capacity of AAV vectors and is associated with Usher syndrome (USH), the most common form of genetic deafblindness. *MYO7A* possesses a functionally equivalent counterpart, *MYO7B*, in humans and in mice fulfilling all requirements

for a replacement of *MYO7A*[31,32]. Following this idea, we first tested single guide (sg)RNAs targeting the region upstream of the *Myo7b* transcriptional start site in 661 W cells, immortalized derivatives of mouse cone photoreceptors, co-transfected with split dCas9-VPR. We identified a combination of sgRNAs that showed efficient activation of *Myo7b* (Fig. S4a–d). To analyze whether *Myo7b* can be activated by dual REVeRT AAVs expressing split dCas9-VPR, we co-transduced primary mouse hippocampal neurons with dual AAV8(Y733F) vectors. This resulted in robust dCas9-VPR reconstitution accompanied by strong *Myo7b* expression (Fig. S4e, f).

The promising in vitro results encouraged us to test whether dual REVeRT AAV vectors are capable of functionally reconstituting dCas9-VPR in vivo under more challenging conditions. As a read-out for dCas9-VPR function, we analyzed the activation of *Myo7b* using the sgRNAs identified in 661 W cells. For this purpose, adult WT mice were subretinally injected with dual REVeRT AAV8(Y733F) vectors (Fig. 3a, b). Four weeks after injection, we observed a strong activation of *Myo7b* at transcript and protein levels (Fig. 3c–e). Next, we tested the same AAV vectors in other organs using different routes of administration. A stereotactic injection into the hippocampus of adult WT mice also resulted in robust activation of the *Myo7b* gene four weeks after injection (Fig. 3f, g). In both retina and hippocampus, the *Myo7b* expression correlated with the dCas9-VPR reconstitution efficiency, suggesting a dose dependency of the transactivation (Fig. S4g, h). We also observed efficient activation of *Myo7b* in several organs (retina, heart, liver, skeletal muscle, and lung) after intraperitoneal injection of these vectors (Fig. 3h, i). Notably, the highest gene activation was detectable in the heart. This is in line with our results from the luciferase assay, which shows the highest REVeRT-mediated luminescence in this organ.

Taken together, these results demonstrate that the REVeRT technology results in functional reconstitution of dCas9-VPR in vivo, irrespective of the administration route.
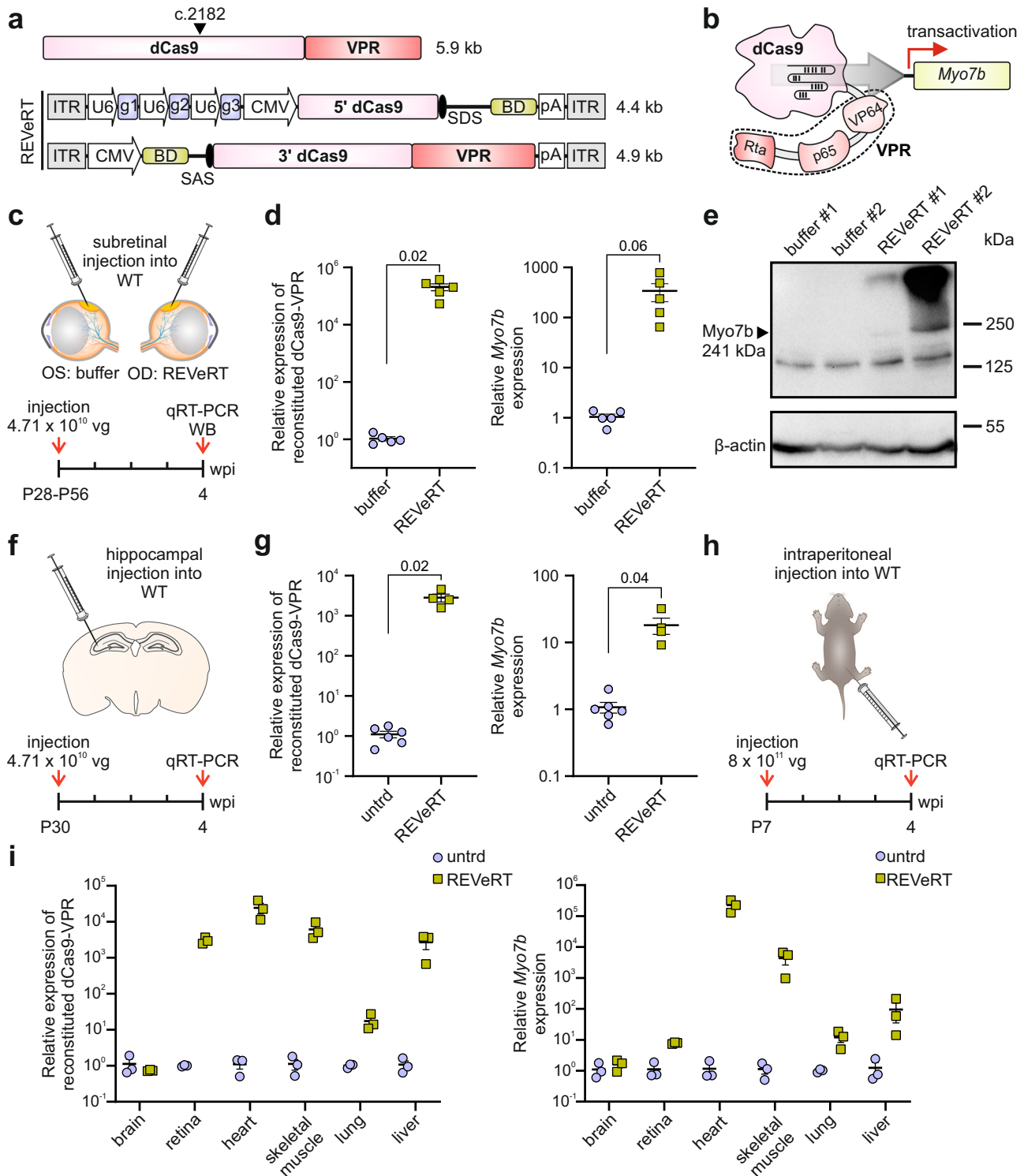
Fig. 3 | Reconstitution of dCas9-VPR in various tissues in vivo upon local and systemic application. a Upper panel, dCas9-VPR size and the split site used for REVeRT. Lower panel, REVeRT vector cassettes expressing split dCas9-VPR and three sgRNAs (g1–g3) targeting the promoter region of *Myo7b*. Titer-matched dual REVeRT AAV8(Y733F) vectors were injected via different routes of administration shown in (**c**, **f**, **h**). **b** dCas9-VPR targeting the *Myo7b* promoter. **c** Experimental design for (**d**, **e**). OD, *Oculus dexter*; OS, *Oculus sinister*. Contralateral eyes injected with AAV formulation buffer served as reference. **d** qRT-PCR from injected retinas. Shown are the relative expression levels of reconstituted dCas9-VPR (left) and the transactivated *Myo7b* (right). $n = 5$ retinas. **e** Western blot from the retinas of two

mice (#1 and #2) injected with REVeRT AAVs or buffer. **f** Experimental design for (**g**). **g** qRT-PCR from injected hippocampi. Shown are the relative expression levels of reconstituted dCas9-VPR (left) and transactivated *Myo7b* (right). Untreated (untrd) hippocampi served as reference. $n = 4$ hippocampi (REVeRT), $n = 6$ hippocampi (untrd). **h** Experimental design for (**i**). **i** qRT-PCR from organs or tissues harvested from intraperitoneally injected mice. Shown are the relative expression levels of reconstituted dCas9-VPR (left) and transactivated *Myo7b* (right). Untreated organs served as reference. $n = 3$ organs/tissues. A two-tailed unpaired t test with Welch's correction was used in (**d**, **g**). Scatter plots show mean ± SEM. All source data in this figure are provided as a Source Data file.

REVeRT leads to functional reconstitution of prime editors in vitro

In addition to CRISPRa, prime editors (PEs) represent another CRISPR-Cas module that exceeds the packaging capacity of AAVs (Fig. S5a) and has high translational potential[33,34]. With the goal of developing dual REVeRT AAV vectors that can reconstitute PEs in vivo, we first attempted to edit the mouse *Dnmt1* locus using previously published prime editing guide (peg) RNAs[33]. Nevertheless, even when expressing the full-length prime editor in transfected 661 W cells, no editing of this locus was detectable under these conditions (Fig. S5b). Similarly, in our attempts to modify other mouse genes (*Rho*, *Cnga1* or *Ush2a*) under different conditions, e.g., in the presence of full-length PE2 and PE3[33], different pegRNAs, or different murine cell lines, we did not detect editing of these loci (Fig. S5b). This prompted us to analyze prime editing of the intergenic human *HEK3* locus using published pegRNAs designed to insert CTT[33]. When the full-length PE2 was expressed in HEK293T cells using calcium phosphate-based transfection, we observed an editing efficiency of 18 %, which is comparable to previously reported results[33]. Next, we co-expressed dual REVeRT PE2 in HEK293T cells. The resulting editing efficiency (16 %) was similar to that of full-length PE2 (Fig. S5c). Moreover, we were able to detect reconstituted PE protein via western blotting (Fig. S5d). This demonstrates that REVeRT is able to functionally reconstitute another therapeutically relevant CRISPR-Cas module in vitro.

In vivo multiplexing for simultaneous gene knockout and activation using dual REVeRT AAVs

It has recently been shown that catalytically active Cas9-VPR can be used for simultaneous activation and knockout of different genes. This is based on the finding that Cas9 loses its catalytic activity in combination with short (<16 nt) sgRNA spacers[35,36]. Consequently, concurrent knockout and activation (hereafter referred to as CONNACT) of different genes can be achieved by combining sgRNAs of different spacer lengths targeting the respective loci. Here, we investigated whether REVeRT is suitable for such multiplexing approaches. One application for CONNACT is the treatment of gain-of-function mutations, which require an efficient knockdown of the diseased allele and the supplementation of another gene to compensate for the missing function. Gain-of-function mutations are frequently found in the rhodopsin gene (*RHO*), including the most common Pro23His (P23H) substitution, and have been associated with retinitis pigmentosa[37]. Moreover, it has recently been shown that transactivation of the M-opsin-encoding gene (*Opn1mw*) can compensate for the lack of rhodopsin function in a mouse model of retinitis pigmentosa[15]. In an attempt to develop a multiplexing approach targeting such mutations, we used dual REVeRT AAV8(Y733F) vectors expressing split Cas9-VPR to simultaneously knockout *Rho* and activate *Opn1mw*. For this purpose, we first tested several different 15 nt spacer sgRNAs targeting the region upstream of the *Opn1mw* transcriptional start site in mouse embryonic fibroblasts (MEFs) (Fig. S5e, f). Notably, in contrast to the results of a recent study targeting other genes[35], we found that 15 nt spacer sequences consistently lead to a decrease in transactivation efficiency compared to their 20 nt counterparts (Fig. S5g).

The CONNACT strategy allows for two parameters of Cas9 functionality (gene activation and knockout) to be analyzed within the same cells. We concluded that such an experimental setup is best suited to compare the efficiency of REVeRT and split-intein-mediated reconstitution in vivo. Therefore, adult WT mice were injected with the dual REVeRT or split-intein AAV cassettes containing one sgRNA with a 20 nt spacer (g1) for *Rho* knockout and the two sgRNAs with a 15 nt spacer (g2 + g3) for *Opn1mw* transactivation (Fig. 4a, b). Four weeks after injection, both, gene knockout and gene activation, were detected in the injected retinas and there were no obvious differences in efficiency when comparing REVeRT and split inteins (Fig. 4c). Next, we evaluated this multiplexing approach in the P23H mouse model of autosomal

dominant retinitis pigmentosa by injecting dual REVeRT AAV vectors subretinally into heterozygous *Rho*[P23H/+] mice. In this context, we also investigated whether the transactivation efficiency could be further increased by adding another *Opn1mw*-targeting sgRNA (g4) to the expression cassette. Four weeks post-injection, both, *Rho* knockdown and *Opn1mw* transactivation, were detected at the transcript and protein level (Fig. 4d, e). The introduction of a third sgRNA targeting *Opn1mw* resulted in a slight increase in activation efficiency (Fig. 4d). The achieved 2-3-fold increase in *Opn1mw* falls short of the previously attained and therapeutically relevant 4-8-fold increase[15] and further assessment is required to determine the minimal and/or optimal *Opn1mw* activation efficiency in *Rho*[P23H/+] mice. RNA-Seq of the injected retinas confirmed the *Opn1mw* activation and *Rho* knockdown (Fig. S5h) and revealed that only a small fraction of additional genes was up- or downregulated under these conditions (Table S3).

Despite being a rare phenomenon, mRNA trans-splicing can also occur between endogenous mRNA molecules in mammalian cells[38,39]. It is therefore conceivable that REVeRT fragments expressed by individual AAVs can be trans-spliced with endogenous transcripts via the donor or acceptor splice sites they contain. To examine the frequency of such trans-splicing events with endogenous transcripts, we analyzed in more detail the RNA-Seq data from the CONNACT (*Rho* and *Opn1mw* sgRNAs) and the corresponding control experiment (*lacZ* sgRNA) described above. To distinguish between target-specific and unspecific effects, we performed each analysis separately. In doing so, we determined which percentage of the total pool of detected transcripts containing either the last or the first nucleotides of the 5' or 3' Cas9 fragments, respectively, were derived from trans-splicing events with annotated endogenous transcripts (Fig. S5i).

We were indeed able to detect splicing with endogenous transcripts in both, the CONNACT and control experiment (Fig. S5j). However, as expected, these events were very rare (94 out of a total of 3175 Cas9-containing sequences for CONNACT (2.96 %) vs. 16 out of a total of 5401 (0.30 %) Cas9-containing sequences in the control experiment). Interestingly, we detected not only numerical but also qualitative differences between the CONNACT and the control experiments. Most strikingly, we detected a much higher rate of transcripts in the CONNACT approach in which the Cas9 fragment was spliced to one of the two target genes (*Rho* or *Opn1mw*). In comparison, only one splicing event involving the *Rho* transcript and none involving the *Opn1mw* transcript were detected in the control experiment using a *lacZ* sgRNA. The most likely explanation for this observation is that the AAV sequences were inserted into the corresponding Cas9 target site in the genome as described in previous studies[40] and subsequently joined together during the regular cis-splicing process with the downstream part of the endogenous transcript. By comparison, in the control *lacZ* sgRNA experiment, the splicing events fusing the exogenous Cas9 transcript with endogenous transcripts most probably arise from "true" trans-splicing itself. Overall, these data suggest that REVeRT-mediated trans-splicing with endogenous transcripts is rather negligible with no enrichment of specific off-target transcripts.

Delivery of full-length ABCA4 into a mouse model of Stargardt disease using dual REVeRT AAVs

Finally, we evaluated the potential of dual REVeRT AAV vectors in the context of gene supplementation therapy. For this, we focused on the Abca4-deficient (*Abca4*^{-/-}) mouse model for Stargardt disease, which represents the most common inherited macular degeneration[41]. To date, no therapy for ABCA4-related Stargardt disease exists, although both split-intein and DNA trans-splicing have been evaluated for their therapeutic potency in mouse models and pigs[12,13,42,43]. The *Abca4*^{-/-} mouse model shows only a mild retinal phenotype[44], which complicates the efficacy evaluation of gene therapies. However, disease progression is enhanced in mice lacking Rdh8 in addition to Abca4[45,46]. To determine the optimal injection time point, we first characterized
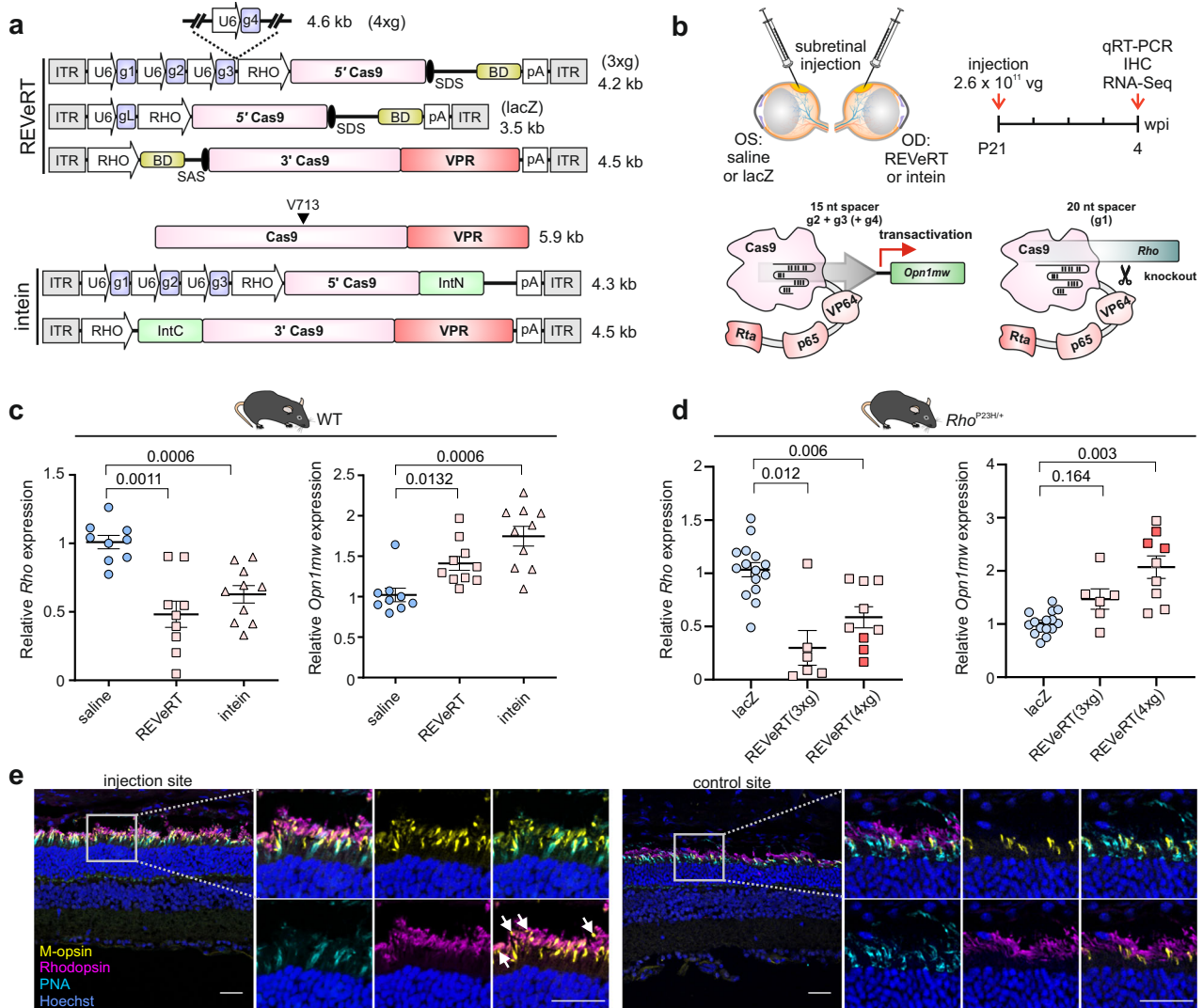
Fig. 4 | Simultaneous gene knockout and transactivation using REVeRT.
a Upper panel, Dual REVeRT AAV8(Y733F) vector cassettes expressing split Cas9-VPR and three sgRNAs targeting either exon 1 of *Rho* (g1) or the promoter region of *Opn1mw* (g2–g4). A *lacZ*-targeting sgRNA (gL) is used as a non-targeting control. Lower panel, The corresponding dual split intein AAV8(Y733F) vector cassettes used for side-by-side comparison to REVeRT shown in (**c**). **b** Experimental design and timeline of experiments shown in c-e. sgRNAs with different spacer lengths are used for a simultaneous knockout (20 nt, g1) of *Rho* and transcriptional activation (15 nt, g2-g4) of *Opn1mw*. g4 was added in (**d**) as indicated. **c** Relative expression of *Rho* and *Opn1mw* in retinas of subretinally injected WT mice. Saline-injected retinas served as a reference. $n = 9$ retinas (saline, REVeRT), $n = 10$ retinas (intein). **d** Relative expression of *Rho* and *Opn1mw* upon subretinal injection of *Rho*^P23H/+ mice with dual REVeRT vectors expressing g1 and either two (REVeRT(3xg)) or

three (REVeRT(4xg)) *Opn1mw* transactivating sgRNAs. Retinas injected with dual REVeRT vectors expressing a *lacZ*-targeting sgRNA served as a reference. The three retinas used for RNA-Seq analysis (Fig. S5h) are shown in dark pink. $n = 15$ retinas (saline), $n = 6$ retinas (REVeRT(3xg)), $n = 9$ retinas (REVeRT(4xg)). Welch's ANOVA with Dunnett T3 was used in c and d. **e** Immunostainings of retinal cryosections of *Rho*^P23H/+ mice subretinally injected with REVeRT(3xg) (left). A control site distal from the injection site is shown as a reference (right). Magnification of areas marked by white rectangles are shown. Arrowheads indicate rod outer segments expressing M-opsin while lacking rhodopsin signal. Peanut agglutinin lectin (PNA) served as a cone outer segment marker. In the control site, M-opsin is only expressed in cones. Scale bar: 30 μm. Scatter plots show mean ± SEM. All source data are provided as a Source Data file.

the retinal degeneration in this *Abca4*^-/-*Rdh8*^-/- mouse model over a period of three months. Using optical coherence tomography (OCT) and electroretinography (ERG), we detected the strongest retinal degeneration between postnatal week (PW) 3 and 5 (Fig. S6a, b). To investigate whether REVeRT can restore full-length ABCA4 protein expression in this mouse model, four animals were injected at PW2 with dual REVeRT AAVs expressing split *ABCA4* (Fig. 5a, b). We chose an intravitreal injection using the recently described AAV2.GL capsids[47]. Although intravitreal injections are a more challenging route of administration as AAVs must overcome additional barriers to reach photoreceptors, this type of injection is therapeutically attractive as it is less invasive and requires less technical skill or specialized equipment[48] than subretinal injections. Four weeks post-injection, no

differences could be seen between the injected and control eyes in ERG or OCT measurements (Fig. S7a, b). Ten weeks after injection, following ERG and OCT measurements (Fig. S7c, d), we analyzed ABCA4 protein expression and localization by western blotting or immunohistochemistry. In three of four injected retinas, full-length ABCA4 protein was present. It was correctly localized in immunolabeled retinal sections (mouse #1) and clearly detected via western blotting (mice #2-3) (Fig. 5c–e, S7e). For mouse #4, no ABCA4 protein was detectable via immunostaining. Similarly, no ABCA4 protein signal was detectable in buffer-injected contralateral control eyes (Fig. 5c). Notably, protein expression data correlated well with ERG and OCT results from the same eyes. In this preliminary experiment, we observe a non-significant trend of improvement in retinal structure and
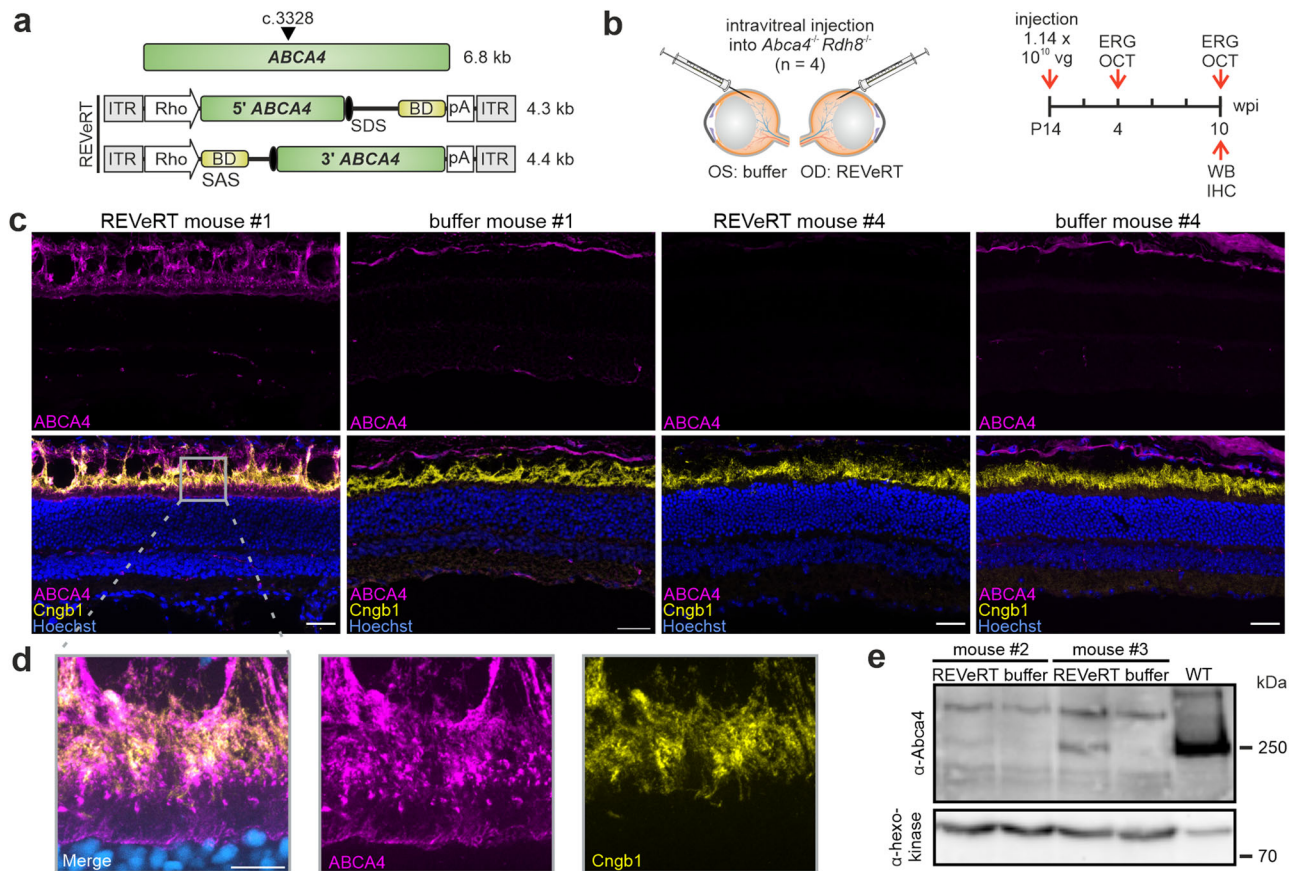
Fig. 5 | ABCA4 reconstitution and full-length protein expression in a Stargardt mouse model using REVeRT. a Upper panel, *ABCA4* size and the split site (arrowhead). Lower panel, Dual REVeRT AAV.GL vectors expressing split *ABCA4*. **b** Experimental design for (**c–e**) and Fig. S7. **c** Representative immunostainings on retinal sections of mouse #1 (left) and mouse (#4) showing a strong or weak improvement in OCT and ERG measurements, respectively. Images of the right eye injected with dual REVeRT AAVs and images of the contralateral control eye injected with buffer solution are shown. Scale bar: 30 µm. Cyclic nucleotide-gated channel (Cngb1) antibody was used as a rod outer segment marker to evaluate ABCA4 localization. Some unspecific ABCA4 staining was detected across all sections above the outer segments. **d** Higher magnification of the area marked by a gray rectangle in (**c**). Scale bar: 10 µm. **e** Western blot from retinas of mouse #2 and mouse #3.

function in eyes of mice #1-3 compared to the contralateral control eyes injected with the AAV formulation buffer (Fig. S7c, d; Fig. S8a–d). Accordingly, mouse #4 showed low to no improvement in ERGs and OCTs.

To get a better understanding of the REVeRT reconstitution efficiency in this therapeutically relevant context, we injected adult *Abca4$^{-/-}$Rdh8$^{-/-}$* mice intravitreally with dual REVeRT AAVs expressing split ABCA4 under (1) an *RHO* promoter specific for rod photoreceptors or (2) a *GRK1* promoter expressed in both photoreceptor types. Four weeks post-injection, we performed a qRT-PCR and analyzed the expression levels of the 5′ part of ABCA4, the 3′ part of ABCA4 and of reconstituted ABCA4 transcript using splice site-spanning primers. We calculated the reconstitution efficiency by determining the ratio of reconstituted ABCA4 transcript relative to the amount of 3′ABCA4 mRNA, which was expressed at lower levels compared to its 5′ ABCA4 counterpart. Under these conditions, the average reconstitution efficiency amounts to $64.3 \pm 15.5\%$ for the *RHO* and $34.0 \pm 0.8\%$ for the *GRK1* promoter (Fig. S8e).

These results demonstrate that the dual REVeRT AAV technology leads to the reconstitution and correct localization of a therapeutically relevant large gene upon intravitreal injection.

Discussion

In this study, we developed a versatile and efficient dual AAV vector technology termed REVeRT that is based on mRNA trans-splicing. We show that REVeRT can be used for functional reconstitution of CRISPRa and prime editors as well as for supplementation of disease-associated genes exceeding the genome packaging capacity of AAVs. In the retina, REVeRT operates at similar efficiencies as split inteins, which are currently the most efficient dual AAV vector approach used in several therapeutically relevant studies[11,12,14]. However, REVeRT offers at least three decisive advantages over split inteins from a scientific and therapeutic perspective: (i) It shows higher flexibility in the split site selection. (ii) The efficiency of reconstitution is less dependent on the position of the split site because it occurs at the transcript level and therefore does not require proper protein folding prior to reconstitution. (iii) It does not generate bacterial proteins, reducing the risk of immune responses in treated individuals. Expression of bacterial proteins such as Cas in CRISPR-based approaches may already trigger immune responses in treated individuals[14,49]. The presence of additional bacterial proteins (e.g., inteins) could result in additive or even synergistic effects potentially heightening the danger of excessive immune reactions. Moreover, in contrast to the split intein approach, REVeRT-mediated reconstitution of genes does not rely on the constant expression of protein fragments. Although no substantial amounts of truncated proteins were detected under the conditions tested herein, we cannot exclude that this might occur in higher frequencies depending on the individual gene to be reconstituted. To minimize the risk of such phenomena, the corresponding REVeRT sequences can be modified, e.g., by removing the polyadenylation signal in the 5′ vector or by shifting the split site to remove potential start codons from the beginning of the 3′ vector's coding sequence.

Among the various CRISPR-Cas techniques, CRISPRa is particularly attractive for therapeutic applications as it is mutation-independent and causes very little off-target effects[50–52]. This strategy was successfully applied in several preclinical studies to treat acquired or genetic disorders such as obesity, acute kidney injury, diabetes mellitus, muscular atrophy, retinitis pigmentosa, or epilepsy[15,50–53]. One of the most powerful CRISPRa modules is Cas9-VPR[29], which is too large to fit into a single AAV vector. REVeRT is capable of functionally reconstituting full-length Cas9-VPR in various therapeutically relevant tissues and organs (i.e., retina, heart, lung, liver, skeletal muscle and brain) and by different routes of application. Cas9-VPR enables the activation of genes which require high expression to achieve a therapeutic effect and is therefore superior over other less efficient CRISPRa modules (e.g. (Sa)Cas9-VP64[54,55]) which are small enough to be delivered with a single AAV strategy[51,52]. In addition, we provide proof of principle that REVeRT can be used efficiently for in vivo multiplexing CRISPR-Cas-based approaches aiming at concurrent knockout and activation of different genes. Such approaches enable the treatment of more complex genetic or acquired diseases. These include genetic disorders caused by gain-of-function mutations as demonstrated in this study. Moreover, the CONNACT strategy could also provide a platform for the treatment of other disorders involving multiple genes or pathways such as cancer or neurodegenerative diseases. For example, REVeRT in combination with CONNACT could be used to knockdown oncogenic genes with simultaneous activation of tumor suppressor genes, or to activate neuroprotective genes with knockdown of cell-damaging or proapoptotic genes. However, when utilizing *Rho*- and *Opn1mw*-targeting sgRNAs simultaneously, we observed the integration of AAV genome into both target sites, albeit to a small extent. The incorporation of AAV sequences into the *Opn1mw* locus indicates that the 15nt spacer sequences do not completely suppress the nuclease activity of *Sp*Cas9 which makes further optimization necessary. The potential effects of such integration events need to be thoroughly investigated for the use of CONNACT as well as other studies employing a catalytically active Cas9.

As REVeRT functions efficiently in different tissues or organs even after intraperitoneal application, it could allow for more convenient treatment of affected individuals for a given disease, e.g., if local administration routes are inappropriate or if multiple organs have to be transduced simultaneously. Nevertheless, although yielding highly promising results in terms of efficacy, further safety parameters such as tolerability, toxicity, or immunoreactivity need to be investigated in non-human primates before REVeRT can be used in clinical trials. Finally, we show that REVeRT works efficiently after intravitreal injections in the context of classical gene supplementation designed to treat one of the most common genetic blinding diseases caused by mutations in the large *ABCA4* gene. We have obtained preliminary experimental data suggesting improvement of retinal degeneration and function in a Stargardt mouse model using the dual REVeRT vector technology in a small cohort of mice. However, a larger cohort of animals and additional functional measurements are needed to fully evaluate the therapeutic effect of this technology for Stargardt gene therapy. In addition to *ABCA4*, there are many other genes that lead to frequent genetic diseases but exceed the capacity of AAVs. These include genes associated with other diseases of the retina (e.g., Usher syndrome or congenital stationary night blindness), the musculature (e.g., Duchenne muscular atrophy), the hematopoietic system (e.g., hemophilia A), the heart (e.g., catecholaminergic polymorphic ventricular tachycardia), but also multisystem disorders such as Timothy syndrome.

Methods

Ethical statement
Animal procedures were performed with permission from local authorities (District Government of Upper Bavaria, Germany) in accordance with the German laws on animal welfare (Tierschutzgesetz).

Mice
Mice were maintained in a 12-h dark/light cycle at an ambient temperature of 22 °C, and 60 % humidity. P0 pups were euthanized by decapitation for hippocampal primary neuron preparation. Adult mice were anesthetized with isoflurane and euthanized by cervical dislocation for organ harvest or decapitation for hippocampi isolation. C57BL/6 J WT mice, *Rho*⁺/P23H (B6.129S6(Cg)-*Rho*^tm1.1Kpal/J, Jackson Laboratory, RRID:IMSR JAX:017628) mice or *Abca4*⁻/⁻ *Rdh8*⁻/⁻ (B6;129-*Abca4*^tm1Ght *Rdh8*^tm1Kpal/J, Jackson Laboratory, RRID:IMSR JAX:030503) mice homozygous for the Leu450 polymorphism in *Rpe65* were used as indicated.

sgRNA/pegRNA design
sgRNAs were designed as described previously[15] using CRISPOR (http://crispor.tefor.net/). pegRNAs were designed using the pegFinder (http://pegfinder.sidichenlab.org/[56]) for targeting *Rho* exon 1, *Ush2a* exon 12, and *Cnga1* exon 9. For *Dnmt1* exon 1 and the human intergenic *HEK3* locus, previously published pegRNAs were used[33]. sgRNA and pegRNA sequences are shown in Table S5 and Table S6.

Cloning
The pAAV.CMV.Luc.IRES.EGFP.SV40, dCas9-VPR, pSMVP-Cas9N, pSMVP-Cas9C, pAAV-CMV-Cas9C-VPR, and pCMV-PE2 plasmids were obtained from Addgene (#105533, #63798, #80934, #80939, and #80933, #132775). REVeRT-based reporter genes, (d)Cas9-VPR, PE2 and ABCA4 constructs were synthesized (BioCat GmbH) and cloned into an ITR-containing plasmid (pAAV2.1). The luciferase constructs were generated using the pAAV.CMV.Luc.IRES.EGFP.SV40 plasmid and cloned into pAAV2.1. Binding domains and splice sites were exchanged, promoter and pA signal removed and sgRNA expression cassettes added[32] using standard cloning techniques. All constructs were sequenced before use (Eurofins Genomics).

Prediction of splice site strength
NNSplice (Berkeley Drosophila Genome Project, http://www.fruitfly.org/seq_tools/splice.html) and the alternative splice site predictor (ASSP, http://wangcomputing.com/assp/) were used. All used splice sites received high splice site prediction scores (0.91-1.0 for NNSplice and 9.2-4.4 for ASSP). Additional information about the sequence composition, polypyrimidine tract, and branch point of the extraordinarily strong splice acceptor site used in this study can be found in our previous study[25].

Cell culture and transfection
HEK293 cells (DMSZ, ACC 305) and HEK293T cells (Takara, 632180) were maintained in Dulbecco's modified Eagle's medium (DMEM) GlutaMAX™ (Thermo Fisher Scientific, high glucose for HEK293T) supplemented with 10% FBS (Biochrom) and with 1% penicillin/streptomycin (P/S, Biochrom) at 37 °C, 10% CO₂. The murine retinoblastoma-derived 661 W cell line was provided by M. Al-Ubaidi[57] and cultured in DMEM GlutaMAX™ medium (with pyruvate) supplemented with 10 % FBS and 1 % Anti-Anti (Thermo Fisher Scientific) at 37 °C, 5% CO₂. Immortalized MEF cells were generated as described previously[58,59] and cultured in DMEM GlutaMAX™ medium supplemented with 10 % FBS and 1% P/S at 37 °C, 5% CO₂. HEK293, HEK293T cells were transfected using the standard calcium phosphate technique. 661 W cells were transfected with the calcium phosphate technique or the Xfect™ transfection reagent (Takara). MEF cells were transfected using TurboFect™ Transfection Reagent (Thermo Fisher Scientific) or the Xfect™ transfection reagent. For co-transfections, equimolar amounts of each plasmid were used. Cells were harvested 48 h post-transfection.

Primary neuron preparation and transduction
The preparation of the hippocampus and isolation of primary hippocampal neurons was done as described previously[60]. The primary neuron culture was maintained at 37 °C and 5 % CO₂ with fresh medium

provided every 2–3 days. Cultivation medium consists of 1% P/S, 1% GlutaMAX™-I and 20 % B27 Supplement in Neurobasal A medium. Primary neurons were transduced at seven days in vitro by adding 7.5×10^{10} vg of titer-matched REVeRT AAV8(Y733F) vectors to the media. Neurons were harvested seven days post-transduction in cell lysis buffer (RLT+ buffer (Qiagen) + 1 % β-mercaptoethanol (Merck)).

AAV production and subretinal/intravitreal injections

REVeRT dual AAV vectors were produced using either the AAV8(Y733F)[28], AAV9 or AAV2.GL capsid[47] as described previously[32]. For subretinal and intravitreal injections, WT, $Rho^{P23H/+}$ and $Abca4^{-/-}Rdh8^{-/-}$ mice were anaesthetized by intraperitoneal injection of 0.02 mg/g body weight ketamine and 0.04 mg/g body weight xylazine and the pupils were dilated using 1% atropine and 0.5% tropicamide eyedrops. Subretinal injections were performed with a NANOFIL 10 μl syringe (World Precision Instruments) and a 34 G beveled needle (World Precision Instruments). For the reconstitution of fluorophores, WT mice were subretinally injected at P21 with 1 μl of dual titer-matched AAV8(Y733F)-split-fluorophore (1.2×10^{12} vg/μl) vectors. For the reconstitution of luciferase, 6-week-old WT mice were subretinally injected with 1 μl of dual titer-matched AAV8(Y733F)-split luciferase (6.0×10^{10} vg/μl) vectors. For transactivation of $Myo7b$, WT mice were subretinally injected at P28-P56 with 1 μl of dual titer-matched AAV8(Y733F)-split-dCas9-VPR (4.71×10^{10} vg/μl) vectors. For multiplexed gene knockout and transactivation, WT and $Rho^{P23H/+}$ mice were subretinally injected at P21 with 1 μl of dual titer-matched AAV8(Y733F)-split-Cas9-VPR (2.6×10^{11} vg/μl) vectors. Contralateral eyes were control injected with 0.9 % NaCl (saline) or phosphate buffer saline containing magnesium and potassium + 0.014% Tween (AAV buffer). To control for Cas9-VPR-specific off-target effects in $Rho^{P23H/+}$ mice, AAVs expressing a $lacZ$-targeting sgRNA were injected into contralateral eyes. Eyes were harvested 4 weeks post-injection. Five $Abca4^{-/-}Rdh8^{-/-}$ mice were injected intravitreally at P14 with 1.5 μl of dual titer-matched AAV2.GL-split-ABCA4 (1.14×10^{10} total vg). The contralateral eyes were control injected with AAV buffer. One mouse was lost during anesthesia in the course of the experiment. Retinas were isolated after final in vivo experiments at 10 weeks post-injection. For the comparison of 5'ABCA4 and 3'ABCA4 expression using different promoters, adult $Abca4^{-/-}Rdh8^{-/-}$ mice were injected intravitreally with AAV2.GL-RHO-split-ABCA4 (6.53×10^{9} total vg per AAV) or with AAV2.GL-GRK1-split-ABCA4 (4.34×10^{9} total vg per AAV). The retinas were processed for RNA extraction four weeks post-injection.

Stereotactic injections

Anesthetized WT mice (P30) were fixed in the stereotactic apparatus in sternal recumbence and the skull was uncovered for bregma and lambda identification. Using the Neurostar software (Neurostar GmbH) bregma and lambda were used as references for calibration. The coordinates for the bilateral injection into the hippocampus were ML ± 1.4, AP -2.06, and DV 1.4. Titer-matched REVeRT AAV8(Y733F) vectors (4.71×10^{10} vg in 0.8 μl) were injected into the hippocampus at a flow rate of 0.3 μl/min. Hippocampi were harvested 4 weeks post-injection.

Intraperitoneal injections

WT mice were injected intraperitoneally at P7 using a 10 μl syringe (Hamilton) and a 28 G beveled needle (Hamilton). For the reconstitution of luciferase, 10 μl of dual titer-matched AAV9 (2×10^{11} vg/μl) vectors were injected. For the reconstitution of dCas9-VPR, 10 μl of dual titer-matched AAV8(Y733F) (8×10^{10} vg/μl) vectors were injected.

Luciferase experiments in vitro and in mice

HEK293T cells were transfected as described above. After 72 h the medium was replaced with 1 ml of culture medium containing 150 mg/ ml luciferin. After a 10 min incubation, the luminescence was measured

on a bioluminescence imaging system (IVIS Spectrum, PerkinElmer). Luminescence images were taken with automatic exposure time, medium binning and F/stop = 1 (Living Image® 4.7.4, PerkinElmer). Three weeks after intraperitoneal injection, 150 mg/kg body weight D-Luciferin (PerkinElmer) were intraperitoneally injected 10-15 minutes prior to imaging. For imaging with the IVIS Spectrum bioluminescence system, the mice were anesthetized with 5% v/v isoflurane in carbogen at 4 L/min. During the measurement, general anesthesia was maintained by mask inhalation of 1.5% v/v isoflurane. Luminescence images were taken with automatic exposure time, medium binning and F/stop = 1 (Living Image® 4.7.4). After imaging, the mice were sacrificed and organs were dissected. Using the luciferase assay system (Promega), the organ-specific luminescence was quantified. Total protein concentration was determined using the Qubit™ Protein and Protein Broad Range (BR) Assay Kit (Invitrogen). The same protocol was used for quantification of luciferase in subretinally injected mouse retinas.

Luciferase experiments in retinal organoids

Human retinal organoids (hROs) were obtained from Newcells Biotech and maintained in the provided culture medium in a round bottom 96-well plate in a CO_2 incubator at 37 °C, 5% CO_2, 20 % O_2. The media was renewed every 3–4 days. For transduction, the culture medium was replaced with 50 μl of medium containing 1.5×10^{12} vg of a single AAV or 3×10^{12} vg of titer-matched dual REVeRT AAV9 vectors expressing the split luciferase. After 7 h, 150 μl medium were added. The medium was changed every 2–3 days thereafter. Seven days after transduction, the medium was replaced with 100 μl of culture medium containing 150 mg/ml luciferin. After 10 min incubation, the luminescence was measured on IVIS Spectrum bioluminescence system. Luminescence images were taken with automatic exposure time, medium binning, and F/stop = 1.

RNA isolation and cDNA synthesis

For RNA extraction from transiently transfected cells, cells were harvested in cell lysis buffer. The retinas were collected as described previously[61]. Retinas and dissected organs (hippocampi, heart, liver, lung, skeletal muscle, and whole brain) were shock-frozen in liquid nitrogen and homogenized in cell lysis buffer using the mixer mill MM400 (Retsch). RNA was extracted using the RNeasy Plus Mini Kit (Qiagen) for transfected cells, primary neurons, retinas, hippocampi, heart, liver, and lung. For primary neurons, additional on-column DNase I digest was performed. For RNA isolation from skeletal muscle, the RNeasy Fibrous Tissue Mini Kit (Qiagen) was used. For RNA isolation from brain tissue, 25 mg of the homogenized lysate was added to 800 μl TRI-Reagent™ (Zymo Research) and homogenized further using the mixer mill MM400 (Retsch) followed by RNA isolation with the Direct-zol™ DNA/RNA Miniprep Kit (Zymo Research). Total RNA concentrations were measured using the Nanodrop™ 2000c spectrophotometer (Thermo Fisher Scientific). Complementary DNA (cDNA) was synthesized using the RevertAid First Strand cDNA Synthesis Kit (Thermo Fisher Scientific) for up to 1 μg total RNA.

(q)RT-PCR

For reverse transcription PCR (RT-PCR), the Herculase II polymerase (Agilent Technologies) was used. Quantitative real-time RT-PCR (qRT-PCR) was performed with duplicates on a MicroAmp™ Fast Optical 96-Well Reaction Plate (Themo Fisher Scientific) using the QuantStudio™ 5 Real-Time PCR system (Thermo Fisher Scientific) and the PowerUp™ SYBR™ Green Master Mix (Themo Fisher Scientific). The expression level of all genes was normalized to $Alas$ except for ABCA4 transcript, which was normalized to $Actb$, and calculated with the $2^{-\Delta\Delta C(T)}$ method. All primers are listed in Table S7. The data was analyzed using the QuantStudioTM Design & Analysis software (Thermo Fisher Scientific).

Protein extraction

For protein extraction from transiently transfected cells, the cells were harvested in TX lysis buffer containing 0.5% Triton-X (v/v), 3% NaCl (5 M, v/v), 0.08% CaCl$_2$ (2.5 M, v/v) and cOmplete™ ULTRA Protease Inhibitor Cocktail tablets (Roche) in H$_2$O. For the Myo7b western blotting, the eyes were removed, punctured with a 21 G needle at the *ora serrata* and incubated in 4% paraformaldehyde (PFA) for 5 minutes before removing the cornea, lens and vitreous body under a stereomicroscope. The eyecup was frozen in liquid nitrogen. For the ABCA4 western blotting, retinas were collected as described above. 100 µl of 1x RIPA lysis buffer (Merck) supplemented with 10 % glycerol and a proteasome inhibitor (Roche) was added. Cells, eyecups, and retinas were disrupted using the mixer mill MM400. The lysates were rotated end-over-end (VWR™ tube rotator) for 20 min (cerulean, Myo7b) or 60 min (ABCA4) at 4 °C and centrifuged.

Western blotting

For western blotting, 15–30 µl of the lysates were incubated in 1x Laemmli sample buffer containing DTT at 72 °C for 10 min. For ABCA4, 30 µl of lysates were incubated with Protein Loading Buffer 5x (National Diagnostics) at 37 °C for 15 min. The proteins were separated on an SDS-polyacrylamide gel via gel electrophoresis. Cerulean and Myo7b blots were stained for 1 h at room temperature (RT) or overnight at 4 °C using the mouse anti-GFP (detects cerulean, 1:2000, JL-8, Clontech, Takara) and the mouse anti-β-tubulin antibody (1:500, D3U1W, Cell Signaling) or with the rabbit anti-Myo7b (1:1000, Sigma-Aldrich) and the mouse anti-β-actin antibody (1:3000, AC-15, Sigma-Aldrich). ABCA4 blots were stained overnight at 4 °C using the rabbit anti-ABCA4 (1:1000, abcam, detecting the C-terminus of the protein) and the rabbit anti-hexokinase II (1:1000, C64G5, Cell Signaling) antibody. Secondary antibodies (Peroxidase AffiniPure anti-rabbit, 1:2000, Jackson, or goat anti-mouse IgG-HRP, 1:2000, Santa Cruz Biotechnology) were added for 1 h at RT. All antibodies used for western blotting have been validated by the manufacturer. The western blots were imaged, and the relative band intensities quantified using the Image-Lab software (Bio-Rad, v5) or VisionWorks LS Analysis Software (for ABCA4, Analytik Jena).

Flow cytometry

Flow cytometry was conducted on HEK293 cells 48 h post-transfection. Cells were detached from the culture plate with TrypLE™ Express (Thermo Fisher Scientific) and centrifuged at $100 \times g$ for 5 min. The pellet was resuspended in 400 µl FACS buffer (2% FBS, 2 mM EDTA (VWR), 25 mM HEPES (Sigma) in PBS), the cells were separated with a 40 µm strainer (pluriSelect) and flow cytometry was performed on a BD LSR Fortessa™ (BD Bioscience) by the Core Facility Flow Cytometry Biomedical Center (LMU Munich). Dead cells were excluded from analysis as determined by SYTOX Blue Dead Cell Stain (Thermo Fisher Scientific). The used gating strategy is shown in Fig. S9.

Fluorescence- (FHC) and immunohistochemistry (IHC)

The eyes were removed and placed in 0.1 M PB. The eyeball was punctured at the ora serrata with a 21 G cannula and fixed in 4 % PFA for 5 min. The cornea, lens, and vitreous body were removed using a stereomicroscope. The eye cup was fixed in 4% PFA for 45 min at RT, cryopreserved in 30 % sucrose solution (w/v) and cryosectioned into 10 µm slices. For FHC, the retina was protected from light during the whole procedure.

For different injections, the retinal sections were stained with different antibodies: mouse anti−rhodopsin 1D4 (1:1500, 1D4, Merck), rabbit anti-M-opsin (1:300, Merck) for detection of native M-opsin in cones and activated M-opsin in rods, mouse anti-ABCA4 (1:100, 3F4, Santa Cruz) and a custom-made rabbit anti-CNGB1 antibody (1:5000) as an outer segment marker. Fluorescein isothiocyanate−conjugated anti-lectin from Arachis hypogaea [peanut agglutinin (PNA)] (1:100,

Sigma-Aldrich, L7381) served as a marker for cones. After overnight incubation at 4 °C, the following secondary antibodies were incubated for 1.5 h at RT: Cy3 anti-rabbit (1:400, Jackson ImmunoResearch), Cy5 anti-mouse (1:400, Jackson ImmunoResearch) and Alexa Fluor Plus 488 anti-mouse (1:800, Thermo Fisher Scientific). All antibodies used for IHC have been validated by the manufacturer. No antibodies were used on FHC sections. For nuclear staining, Hoechst 33342 solution (5 µg/ml, Invitrogen) was incubated for 5 min.

Microscopy

For FHC and Rho^{P23H} IHC retinal sections, z-stack images were obtained using a Leica TCS SP8 inverted confocal laser scanning microscope and the LASX software (Leica). For fluorophore-specific bleaching, a single cell was zoomed in on and the laser intensity of the citrine- and mCherry-specific channels was increased to 80%. For ABCA4$^{-/-}$ IHC sections, z-stack images were acquired with a ZEISS AxioObserver7 imaging platform with ApoTome2. Deconvolution and maximum intensity z-projection were performed in the ZEISS Zen Blue 3.3 Software. Images of transfected living cells were obtained using the Leica TCS SP8 spectral confocal laser scanning microscope equipped with a HCX APO 20x/1.00 W objective (Leica). All images were processed further with the Fiji/ImageJ software (https://fiji.sc, 1.54f, National Institutes of Health).

DNA isolation

Transfected HEK293T, 661 W and MEF cells were harvested in cell lysis buffer. The cells were disrupted using the mixer mill MM400. The lysates were centrifuged at $5000 \times g$ for 10 min at 4 °C and supernatant added to gDNA extraction columns (Zymo Research). The columns were centrifuged for 4 min at $1500 \times g$ and 1 min at $10,000 \times g$ at RT and incubated with 400 µl Genomic lysis buffer (Zymo Research) supplemented with RNase A (Sigma-Aldrich, 1:5000) for 10 min followed by a 2 min centrifugation at RT. 400 µl of DNA Pre-Wash buffer (Zymo Research) and 600 µl of g-DNA Wash buffer (Zymo Research) were added with intermediate centrifugation steps for 1 min at $10,000 \times g$. 600 µl of g-DNA Wash buffer was added again and centrifuged for 2 min at $10000 \times g$. To elute gDNA, 100 µl of H$_2$O were added to the column, incubated for 20 min at RT and centrifuged for 2 min at $10,000 \times g$. gDNA concentrations were measured using the Nanodrop™ 2000c spectrophotometer.

Quantification of prime editing efficiency

For amplification of the respective target locus, 100 ng of the extracted gDNA were for PCR with the Q5 high-fidelity DNA polymerase (New England Biolabs). The product was analyzed via gel electrophoresis, purified from the agarose gel with the QIAquick gel extraction kit (Qiagen) and Sanger sequenced (Eurofins Genomics). To quantify the prime editing efficiency, the PCR was repeated using primers containing Illumina partial adapters (Table S7). The product was purified as described above and sent to next-generation amplicon sequencing (Azenta Life Sciences). Analysis of the amplicon sequencing was performed by Azenta Life Sciences. Briefly, raw reads were trimmed using a sliding window of 20 bases and a minimum average base quality score of 20 in the window. Next, trimmed reads were aligned with the amplicon sequence and filtered for reads spanning the PE target sequence termed "target reads". The editing efficiency was calculated as the ratio of the number of target reads per sample containing the correct edit and the total number of target reads per sample.

RNA-Seq

Total RNA was sent to a commercial provider (Azenta Life Sciences) to perform RNA sequencing and analysis. mRNA was enriched by poly(A) selection. Paired-end sequencing was performed on an Illumina HiSeq system with >20 million reads per sample and 150 bp read length.

Trimmomatic v.0.36 was used to trim the sequence reads for adapter sequences and quality. The reads were mapped to the *Mus musculus* GRCm38 reference genome (Ensembl) using the STAR aligner v.2.5.2b. Unique gene hit counts were calculated using FeatureCounts from the Subread package v.1.5.2 and only unique reads mapped to exonic regions were included. DESeq2 was used to analyze the obtained gene hit counts. The Wald test was used to obtain p-values and log2 fold changes. Differentially expressed genes were defined by an absolute log2 fold change > 1 and adjusted *p*-value < 0.05.

To evaluate splicing with endogenous transcripts in the RNA-Seq data set, RStudio version 2022.07.1 + 554 "Spotted Wakerobin" Release (7872775ebddc40635780ca1ed238934c3345c5de, 2022-07-22) for macOS was used. First, the reads were filtered to contain the sequences directly upstream or downstream of the Cas9-VPR splice site, i.e., gcacatcgctaatcttgcag or gtagcccagctatcaaaaag or their respective reverse complements. All matched sequences were filtered for correct and alignable length (more than 25 nt, less than 149) and for sequencing quality. The sequences were aligned with the TxDb.Mmusculus.UCSC.mm10.knownGene *Mus musculus* genome. All transcripts identified as a fusion between REVeRT transcripts and endogenous transcripts are listed in Table S4.

Electroretinography (ERG)

Mice were dark-adapted overnight. Tropicamide eye drops were applied for pupil dilation (Mydriadicum Stulln, Pharma Stulln GmbH). Full-field ERG responses were recorded using a Celeris apparatus (Diagnosys LLC). Light guide electrodes were placed on each eye. For the scotopic measurements, the eyes were illuminated in single flashes with increasing light intensities (0.003, 0.01, 0.03, 0.1, 0.3, 1, 3, 10 cd.s/m^2). After a 5 min-light adaptation step with 9 cd/m^2, sequential photopic responses were recorded for single-flash steps 0.01, 0.03, 0.1, 0.3, 1, 3, 10 cd.s/m^2 with constant 9 cd/m^2 background illumination. Flicker recordings were performed for 20 and 30 Hz at 3 cd.s/m^2 with constant 9 cd/m^2 background illumination.

Optical coherence tomography (OCT)

OCT was performed with an adapted Spectralis HRA + OCT system (Heidelberg Engineering) in combination with optic lenses using the Heidelberg Eye Explorer software version 1.10.4.0. OCT scans were conducted with a linear scan mode. The mean outer nuclear layer (ONL) thickness was defined as the width of the retinal layer containing the nuclei of rod and cone photoreceptors and was calculated from single values measured in the dorsal, temporal, nasal, and ventral region around the optic nerve.

Statistical analysis and reproducibility

All values are given as mean ± SEM. The number of replicates (n) are stated in the figure legends and can be inferred from scatter plots for each experiment. Statistical analysis was performed using GraphPad PRISM (GraphPad Software, v10.0.2). Normality was tested using a Shapiro-Wilk test. For parametric unpaired data, unpaired *t* test with Welch's correction or Welch's ANOVA was used. For non-parametric unpaired data, Mann–Whitney or Kruskal–Wallis test was used. Multiple comparisons were corrected for using Dunnett's T3 test. Correlation coefficients were calculated using Spearman's correlation. In experiments with paired samples, a paired t-test with Welch's correction or a two-way ANOVA with Šídák's multiple comparisons test were used. All transfections in Fig. 1b have been repeated a minimum of 4 times per binding domain. The RT-PCR shown in Fig. 1c has been repeated twice. The western blot in Fig. 4e has been repeated once. The immunohistochemical staining shown in Fig. 5c, d has been repeated for a minimum of 10 more sections. The western blot shown in Fig. 5e has been repeated once. No statistical method was used to predetermine the sample size. No data were excluded from the analyses. All animals and cells were randomly assigned to the experimental or the control group. The investigators were not blinded to allocation during experiments and outcome assessment.

Reporting summary

Further information on research design is available in the Nature Portfolio Reporting Summary linked to this article.

Data availability

All source data are provided as a Source Data file. The datasets generated in this study are available in public repositories. The RNA-Seq data have been deposited to GEO (Gene Expression Omnibus) under the GEO accession GSE198893 [https://www.ncbi.nlm.nih.gov/geo/query/acc.cgi?acc=GSE198893]. The NGS data from the prime editing experiments have been also deposited to GEO under the GEO accession GSE198863 [https://www.ncbi.nlm.nih.gov/geo/query/acc.cgi?acc=GSE198863]. All final REVeRT sequence elements used in this study are listed in Table S2. Full sequences of the final constructs used for gene therapy experiments are provided in the Supplementary Information. Additionally, sgRNAs, pegRNAs and primers used in this study can be found in Table S5, S6 and S7. The gating strategy used in this study is displayed in Fig. S1. The *Mus musculus* GRCm38 reference genome can be accessed via Ensembl (http://nov2020.archive.ensembl.org/Mus_musculus/Info/Index). Source data are provided with this paper.

References

1. Wang, D., Tai, P. W. L. & Gao, G. Adeno-associated virus vector as a platform for gene therapy delivery. *Nat. Rev. Drug Discov.* **18**, 358–378 (2019).
2. Wang, D., Zhang, F. & Gao, G. CRISPR-based therapeutic genome editing: strategies and in vivo delivery by AAV vectors. *Cell* **181**, 136–150 (2020).
3. Wu, Z., Yang, H. & Colosi, P. Effect of genome size on AAV vector packaging. *Mol Ther.* **18**, 80–86 (2010).
4. van Haasteren, J., Li, J., Scheideler, O. J., Murthy, N. & Schaffer, D. V. The delivery challenge: fulfilling the promise of therapeutic genome editing. *Nat. Biotechnol.* **38**, 845–855 (2020).
5. Trapani, I., Tornabene, P. & Auricchio, A. Large gene delivery to the retina with AAV vectors: are we there yet? *Gene Ther.* **28**, 220–222 (2021).
6. Duan, D., Yue, Y., Yan, Z. & Engelhardt, J. F. A new dual-vector approach to enhance recombinant adeno-associated virus-mediated gene expression through intermolecular cis activation. *Nat. Med.* **6**, 595–598 (2000).
7. Yang, J. et al. Concatamerization of adeno-associated virus circular genomes occurs through intermolecular recombination. *J. Virol.* **73**, 9468–9477 (1999).
8. Patel, A., Zhao, J., Duan, D. & Lai, Y. Design of AAV vectors for delivery of large or multiple transgenes. *Methods Mol. Biol.* **1950**, 19–33 (2019).
9. Ryu, S. M. et al. Adenine base editing in mouse embryos and an adult mouse model of Duchenne muscular dystrophy. *Nat. Biotechnol.* **36**, 536–539 (2018).
10. Carvalho, L. S. et al. Evaluating efficiencies of dual AAV approaches for retinal targeting. *Front. Neurosci.* **11**, 503 (2017).
11. Levy, J. M. et al. Cytosine and adenine base editing of the brain, liver, retina, heart and skeletal muscle of mice via adeno-associated viruses. *Nat. Biomed. Eng.* **4**, 97–110 (2020).
12. Tornabene, P. et al. Intein-mediated protein trans-splicing expands adeno-associated virus transfer capacity in the retina. *Sci. Transl. Med.* **11**, eaav4523 (2019).
13. Trapani, I. et al. Effective delivery of large genes to the retina by dual AAV vectors. *EMBO Mol. Med.* **6**, 194–211 (2014).
14. Chew, W. L. et al. A multifunctional AAV-CRISPR-Cas9 and its host response. *Nat. Methods* **13**, 868–874 (2016).

15. Böhm, S. et al. A gene therapy for inherited blindness using dCas9-VPR-mediated transcriptional activation. *Sci. Adv.* **6**, eaba5614 (2020).

16. Villiger, L. et al. Treatment of a metabolic liver disease by in vivo genome base editing in adult mice. *Nat Med* **24**, 1519–1525 (2018).

17. Lim, C. K. W. et al. Treatment of a mouse model of ALS by in vivo base editing. *Mol Ther* **28**, 1177–1189 (2020).

18. Muralidharan, V. & Muir, T. W. Protein ligation: an enabling technology for the biophysical analysis of proteins. *Nat. Methods* **3**, 429–438 (2006).

19. Shah, N. H. & Muir, T. W. Inteins: nature's gift to protein chemists. *Chem. Sci.* **5**, 446–461 (2014).

20. Song, Y. et al. Functional cystic fibrosis transmembrane conductance regulator expression in cystic fibrosis airway epithelial cells by AAV6.2-mediated segmental trans-splicing. *Hum. Gene Ther.* **20**, 267–281 (2009).

21. Pergolizzi, R. G. et al. In vivo trans-splicing of 5' and 3' segments of pre-mRNA directed by corresponding DNA sequences delivered by gene transfer. *Mol. Ther.* **8**, 999–1008 (2003).

22. Yan, Z., Zhang, Y., Duan, D. & Engelhardt, J. F. Trans-splicing vectors expand the utility of adeno-associated virus for gene therapy. *Proc Natl Acad Sci USA* **97**, 6716–6721 (2000).

23. Reich, S. J. et al. Efficient trans-splicing in the retina expands the utility of adeno-associated virus as a vector for gene therapy. *Hum. Gene Ther.* **14**, 37–44 (2003).

24. Ghosh, A., Yue, Y., Long, C., Bostick, B. & Duan, D. Efficient whole-body transduction with trans-splicing adeno-associated viral vectors. *Mol. Ther.* **15**, 750–755 (2007).

25. Riedmayr, L. M., Bohm, S., Biel, M. & Becirovic, E. Enigmatic rhodopsin mutation creates an exceptionally strong splice acceptor site. *Hum. Mol. Genet.* **29**, 295–304 (2020).

26. Hu, M. L. et al. Gene therapy for inherited retinal diseases: progress and possibilities. *Clin. Exp. Optom.* **104**, 444–454 (2021).

27. Michalakis, S., Gerhardt, M., Rudolph, G., Priglinger, S. & Priglinger, C. Gene therapy for inherited retinal disorders: update on clinical trials. *Klin. Monbl. Augenheilkd* **238**, 272–281 (2021).

28. Petrs-Silva, H. et al. High-efficiency transduction of the mouse retina by tyrosine-mutant AAV serotype vectors. *Mol. Ther.* **17**, 463–471 (2009).

29. Chavez, A. et al. Comparison of Cas9 activators in multiple species. *Nat. Methods* **13**, 563–567 (2016).

30. Becirovic, E. Maybe you can turn me on: CRISPRa-based strategies for therapeutic applications. *Cell Mol. Life Sci.* **79**, 130 (2022).

31. Yu, I. M. et al. Myosin 7 and its adaptors link cadherins to actin. *Nat. Commun.* **8**, 15864 (2017).

32. Riedmayr, L. M. et al. dCas9-VPR-mediated transcriptional activation of functionally equivalent genes for gene therapy. *Nat. Protoc.* **17**, 781–818 (2022).

33. Anzalone, A. V. et al. Search-and-replace genome editing without double-strand breaks or donor DNA. *Nature* **576**, 149–157 (2019).

34. Scholefield, J. & Harrison, P. T. Prime editing—an update on the field. *Gene Ther.* **28**, 396–401 (2021).

35. Kiani, S. et al. Cas9 gRNA engineering for genome editing, activation and repression. *Nat. Methods* **12**, 1051–1054 (2015).

36. Dahlman, J. E. et al. Orthogonal gene knockout and activation with a catalytically active Cas9 nuclease. *Nat. Biotechnol.* **33**, 1159–1161 (2015).

37. Meng, D., Ragi, S. D. & Tsang, S. H. Therapy in rhodopsin-mediated autosomal dominant retinitis pigmentosa. *Mol. Ther.* **28**, 2139–2149 (2020).

38. Chuang, T. J. et al. Integrative transcriptome sequencing reveals extensive alternative trans-splicing and cis-backsplicing in human cells. *Nucleic Acids Res.* **46**, 3671–3691 (2018).

39. Wu, C. S. et al. Integrative transcriptome sequencing identifies trans-splicing events with important roles in human embryonic stem cell pluripotency. *Genome Res.* **24**, 25–36 (2014).

40. Hanlon, K. S. et al. High levels of AAV vector integration into CRISPR-induced DNA breaks. *Nat. Commun.* **10**, 4439 (2019).

41. Piotter, E., McClements, M. E. & MacLaren, R. E. Therapy approaches for stargardt disease. *Biomolecules* **11**, 1179 (2021).

42. Colella, P. et al. Efficient gene delivery to the cone-enriched pig retina by dual AAV vectors. *Gene Ther.* **21**, 450–456 (2014).

43. McClements, M. E. et al. An AAV dual vector strategy ameliorates the stargardt phenotype in adult Abca4(-/-) mice. *Hum. Gene Ther.* **30**, 590–600 (2019).

44. Weng, J. et al. Insights into the function of Rim protein in photoreceptors and etiology of Stargardt's disease from the phenotype in abcr knockout mice. *Cell* **98**, 13–23 (1999).

45. Maeda, A., Golczak, M., Maeda, T. & Palczewski, K. Limited roles of Rdh8, Rdh12, and Abca4 in all-trans-retinal clearance in mouse retina. *Invest. Ophthalmol. Vis. Sci.* **50**, 5435–5443 (2009).

46. Maeda, A., Maeda, T., Golczak, M. & Palczewski, K. Retinopathy in mice induced by disrupted all-trans-retinal clearance. *J. Biol. Chem.* **283**, 26684–26693 (2008).

47. Pavlou, M. et al. Novel AAV capsids for intravitreal gene therapy of photoreceptor disorders. *EMBO Mol. Med.* **13**, e13392 (2021).

48. Dalkara, D. et al. Inner limiting membrane barriers to AAV-mediated retinal transduction from the vitreous. *Mol. Ther.* **17**, 2096–2102 (2009).

49. Hakim, C. H. et al. Cas9-specific immune responses compromise local and systemic AAV CRISPR therapy in multiple dystrophic canine models. *Nat. Commun.* **12**, 6769 (2021).

50. Liao, H. K. et al. In vivo target gene activation via CRISPR/Cas9-mediated trans-epigenetic modulation. *Cell* **171**, 1495–1507 e1415 (2017).

51. Matharu, N. et al. CRISPR-mediated activation of a promoter or enhancer rescues obesity caused by haploinsufficiency. *Science* **363**, eaau0629 (2019).

52. Kemaladewi, D. U. et al. A mutation-independent approach for muscular dystrophy via upregulation of a modifier gene. *Nature* **572**, 125–130 (2019).

53. Colasante, G. et al. dCas9-Based Scn1a gene activation restores inhibitory interneuron excitability and attenuates seizures in dravet syndrome mice. *Mol. Ther.* **28**, 235–253 (2020).

54. Perez-Pinera, P. et al. RNA-guided gene activation by CRISPR-Cas9-based transcription factors. *Nat. Methods* **10**, 973–976 (2013).

55. Maeder, M. L. et al. CRISPR RNA-guided activation of endogenous human genes. *Nat. Methods* **10**, 977–979 (2013).

56. Chow, R. D., Chen, J. S., Shen, J. & Chen, S. A web tool for the design of prime-editing guide RNAs. *Nat. Biomed. Eng.* **5**, 190–194 (2021).

57. al-Ubaidi, M. R. et al. Bilateral retinal and brain tumors in transgenic mice expressing simian virus 40 large T antigen under control of the human interphotoreceptor retinoid-binding protein promoter. *J. Cell Biol.* **119**, 1681–1687 (1992).

58. Jat, P. S., Cepko, C. L., Mulligan, R. C. & Sharp, P. A. Recombinant retroviruses encoding simian virus 40 large T antigen and polyomavirus large and middle T antigens. *Mol. Cell Biol.* **6**, 1204–1217 (1986).

59. Xu, J. Preparation, culture, and immortalization of mouse embryonic fibroblasts. *Curr. Protoc. Mol. Biol.* **Chapter 28**, Unit 28 21 (2005).

60. Fath, T., Ke, Y. D., Gunning, P., Gotz, J. & Ittner, L. M. Primary support cultures of hippocampal and substantia nigra neurons. *Nat. Protoc.* **4**, 78–85 (2009).

61. Becirovic, E. et al. AAV vectors for FRET-based analysis of protein-protein interactions in photoreceptor outer segments. *Front. Neurosci.* **10**, 356 (2016).

Author contributions

Conceptualization, E.B.; Methodology, L.M.R. and E.B.; Investigation, L.M.R, K.S.H., S.B.T., N.K., S.B., D.M.M., V.J.W., D.Y.O., M.D.B., V.S., M.Br., R.F., N.B., G.M.W., and V.M.; Writing—Original Draft, E.B.; Writing—Review & Editing, L.M.R., K.S.H., S.B.T., N.K., V.M., S.M., S.F., and M.Bi.; Visualization, L.M.R., K.S.H., and E.B.; Funding Acquisition, C.G., J.Wi., S.M., S.F., M.Bi., and E.B.; Supervision, J.Wi., V.M., S.M., S.F., M.Bi., and E.B.

Competing interests

L.M.R, S.B., V.S., M.Bi., S.M., and E.B. are authors on a patent application covering transactivation of homologous genes (PCT/EP2020/076536, filed by ViGeneron GmbH, status: published). E.B., M.Bi., and S.M. are authors on a patent application covering the splice site module and its applications (PCT/EP2019/086454, filed by ViGeneron GmbH, status: published). S.M. and M.Bi. are co-founders and shareholders of ViGeneron GmbH and members of its scientific advisory board. E.B. is a member of scientific advisory board of ViGeneron GmbH. The remaining authors declare no competing interests.

Additional information

Supplementary information The online version contains supplementary material available at https://doi.org/10.1038/s41467-023-42386-0.

Correspondence and requests for materials should be addressed to Elvir Becirovic.

Peer review information *Nature Communications* thanks Rasmus Bak, and the other, anonymous, reviewer(s) for their contribution to the peer review of this work.

Reprints and permissions information is available at http://www.nature.com/reprints

Publisher's note Springer Nature remains neutral with regard to jurisdictional claims in published maps and institutional affiliations.